Passive linear nanoscale optical and molecular electronics device synthesis from nanoparticles

Bernard Yurke[1,2,*] and Wan Kuang[2,†]

[1]*Department of Materials Science and Engineering, Boise State University, 1910 University Drive, Boise, Idaho 83725, USA*

[2]*Department of Electrical and Computer Engineering, Boise State University, 1910 University Drive, Boise, Idaho 83725, USA*

(Received 22 September 2009; published 9 March 2010)

Arrays of nanoparticles whose interactions can be characterized by hopping Hamiltonians can serve as excitation transmission lines. Here we show, that in addition suitable arrangements of nanoparticles can form beam splitters, phase shifters, and crossover splitters. With these elements, any discrete unitary transformation can be implemented on input modes via a network of nanoparticles in which all the components lie in the same plane. These nanoparticle networks can produce optical functionalities at a length scale much smaller than 1 μm.

DOI: 10.1103/PhysRevA.81.033814 PACS number(s): 42.79.Gn, 42.82.Et

I. INTRODUCTION

The development of techniques for fabrication at the nanoscale level has made it increasingly easy to fabricate systems consisting of nanoscale components precisely positioned with respect to each other. Such components, properly arranged, could form signal-processing devices and systems with high component density that operate at high speeds. One-dimensional arrays consisting of chromophores, quantum dots, or metal nanoparticles, spaced within nanometers of each other, have been fabricated. Such arrays have been proposed for use as transmission lines to transport electromagnetic energy in the form of plasmons or excitons either by coherent or diffusive means [1,2]. Such light guides can confine electromagnetic energy to length scales smaller than the diffraction limit, a feature that is attractive for high-component-density optical devices. Arrays of nanoparticles or molecules can also serve as wires to transport charge, especially if the particles are strongly coupled through close proximity or via molecular interconnections. A feature in common among these diverse transmission lines is that their signal propagation behavior often can be characterized usefully by hopping Hamiltonians. However, to make signal-processing devices, generally more than transmission lines are needed. Passive linear devices, such as beam splitters and phase shifters, are desired for the construction of devices that transform and route signals among transmission lines. Active and nonlinear devices are also desired for amplification and switching. Construction of such passive and active devices via appropriately spaced nanoparticles has received considerably less attention than that of transmission lines. Here we show how linear passive devices, which can be interconnected via transmission lines, can be constructed via suitable arrangements of nanoparticles or molecular constituents.

A brief summary of prior theoretical and experimental work on passive and active devices based on the arrangement of metal nanoparticles, quantum dots, or chromophores in close proximity to each other is provided here. The coherent propagation of electromagnetic energy via plasmon transmission lines consisting of arrays of metal nanoparticles has been discussed by a number of authors [3–12], and some experimental work has been performed [10]. Electromagnetic energy propagation for the case when the metallic nanoparticle arrays contain corner and T-shaped structures has also been investigated [9,13,14]. Theoretical work on exciton energy transfer between quantum dots has been performed [15–18], and experimental work has been reported on gain-enabled transmission lines consisting of arrays of quantum dots [19,20]. Chromophore-based transmission lines on which exciton energy is diffusively transported via fluorescence resonance energy transfer (FRET) between donor and acceptor dyes [21] have been experimentally investigated [22–24]. The possibility that exciton energy can be coherently propagated between donor and acceptor dyes, provided the chromophores are sufficiently closely spaced, has been theoretically investigated [25–32]. There is substantial experimental evidence that exciton energy is coherently propagated in the light-harvesting complex of photosynthetic organisms [33–35], and transmission lines that propagate exciton energy coherently along an array of chromophores have been devised [36]. Coherent electron transport can also occur between strongly coupled nanoparticles, such as quantum dots [37,38], or between atoms in conjugated hydrocarbon molecules.

In this article, we show how beam splitters and phase shifters can be synthesized from discrete components whose interactions can be described by hopping Hamiltonians. For the case of exciton hopping, these components could consist of chromophores, such as dye molecules, or quantum dots. The propagation of plasmon excitations between metallic nanoparticles is also often adequately described by hopping Hamiltonians, as are electrons propagating from carbon atom to carbon atom in conjugated hydrocarbons. We present a general formalism for the synthesis of linear, passive, lossless devices that is applicable to all of these cases, and we refer to the devices generically as excitation devices. In addition, we show that it is possible to construct crossovers or pass throughs for which all the components lie in the same plane, thereby allowing excitation signals to pass through each other without scattering into each others' channels. Since it is known that any discrete unitary transformation can be implemented via a suitable network of beam splitters and phase shifters [39], these pass throughs allow the construction of such networks in which all the components lie in the same plane. This possibility should greatly simplify the task of fabricating complex passive linear networks.

*bernardyurke@boisestate.edu

†wankuang@boisestate.edu

 ©2010 The American Physical Society

Loss and decoherence are challenging problems for the construction of nanoscale devices. However, we hope that continued improvements in materials and nanofabrication will allow the construction of systems in which coherent effects can outrun decoherence long enough for the work presented here to serve as a useful guide for the engineering of passive linear devices; we do not include such effects in the present analysis.

II. GENERAL FORMALISM

As a way of establishing notation, here we consider the general behavior of systems governed by hopping Hamiltonians. First, consider the Hamiltonian

$$H = \sum_m \hbar\omega_m \hat{\sigma}_m^+ \hat{\sigma}_m^- + \sum_{[m,n]} \hbar g_{mn} (\hat{\sigma}_m^+ \hat{\sigma}_n^- + \hat{\sigma}_n^+ \hat{\sigma}_m^-), \quad (1)$$

which models two-level systems that interchange excitons via a hopping interaction. The first sum on the right is a sum over the Hamiltonians for each individual two-level system. The energy difference between the excited state and the ground state of the mth two-level system is $\hbar\omega_m$. The second sum is over all pairs of two-level systems that interact via a hopping interaction. The strength of the hopping interaction between the mth and nth two-level system in energy units is $\hbar g_{mn}$. Letting $|g_m\rangle$ and $|e_m\rangle$ denote, respectively, the ground state and the excited state of the mth two-level system, the operators σ_m^+ and σ_m^- are given by

$$\hat{\sigma}_m^+ = |e_m\rangle\langle g_m| \quad (2)$$

$$\hat{\sigma}_m^- = |g_m\rangle\langle e_m|. \quad (3)$$

Since the Hamiltonian conserves exciton number, the Hamiltonian block diagonalizes according to exciton number. Here we restrict our attention to the single-particle sector of the Hilbert space; that is, we consider the case where a single exciton hops from two-level system to two-level system. Let $|0\rangle$ denote the state for which all the two-level systems are in their ground state. Then an arbitrary state vector in the single-exciton sector can be written in the form

$$|\psi\rangle = \sum_m \alpha_m \hat{\sigma}_m^+ |0\rangle, \quad (4)$$

where α_m is the probability amplitude that the mth two-level system is excited. Equations (1) and (4), substituted into the Schrödinger equation,

$$i\hbar \frac{\partial}{\partial t}|\psi\rangle = H|\psi\rangle, \quad (5)$$

yields the following differential equation for the probability amplitude $\alpha_m(t)$:

$$i\frac{d\alpha_m}{dt} = \omega_m \alpha_m + \sum_n g_{mn}\alpha_n. \quad (6)$$

Before proceeding with device synthesis using Eq. (6), it is worth noting several other contexts in which such an equation arises. Consider the Hamiltonian

$$H = \sum_m \hbar\omega_m \hat{a}_m^\dagger \hat{a}_m + \sum_{[m,n]} \hbar g_{mn} (\hat{a}_m^\dagger \hat{a}_n + \hat{a}_n^\dagger \hat{a}_m) \quad (7)$$

where $\hat{a}_m$ is an annihilation operator. For the moment, we leave unspecified whether it is a boson or fermion annihilation operator. A state vector in the single-particle sector has the general form

$$|\psi\rangle = \sum_m \alpha_m \hat{a}_m^\dagger |0\rangle. \quad (8)$$

Equation (6) is applicable to fermion systems, such as electrons hopping from carbon atom to carbon atom in conjugated hydrocarbon molecules.

It is also applicable to boson systems, such as plasmon excitations hopping from metal particle to metal particle. The electromagnetic energy transport among metal nanoparticles relies on the near field interaction between metal particles that can be approximated by coupled dipole modes. The lossless interaction between closely spaced dipoles can be described by the equation of motion [14,40],

$$\frac{d^2 p_m}{dt^2} = -\omega_0^2 p_m - \sum_n \omega_{mn}^2 p_n, \quad (9)$$

where p_m is the oscillating dipole moment at a point m in the chain and ω_{mn}^2 is the coupling strength between the adjacent dipoles m and n. The energy relaxation due to interactions with phonons and impurity is ignored as well as the energy relaxation due to the radiation into the far field. Equations (6) and (9) differ only in their relationship with the resonant frequency ω_0. It is worth noting that by introducing

$$a_m = \sqrt{\frac{\omega_m}{2\hbar}} \left(\frac{i}{\omega_m}\frac{dp_m}{dt} + p_m \right), \quad (10)$$

Eq. (9) can be expressed as

$$\frac{da_m}{dt} = -i\omega_m a_m - \frac{i}{2}\sum_n \frac{\omega_{mn}^2}{\sqrt{\omega_m \omega_n}} a_n \quad (11)$$

when the coupling is much smaller than the characteristic dipole osicllation frequency. Note that Eq. (11) has the same form as Eq. (6).

Equation (6) also has relevance in the many-particle sector provided particle-particle interactions are unimportant. A boson many-body case particularly worthy of note is that for which the state vector $|\psi\rangle$ consists of a product of coherent states,

$$|\psi\rangle = \prod_m |\alpha_m\rangle, \quad (12)$$

where

$$|\alpha_m\rangle = e^{-|\alpha_m|^2} e^{\alpha_m \hat{a}^\dagger} |0\rangle \quad (13)$$

is the coherent state for the mth site and α_m is the mean field at this site. This state vector is a solution of the Schrödinger equation, Eq. (5), provided Eq. (6) is satisfied. As a consequence, Eq. (6) is also applicable to classical electromagnetic field modes, such as coherently excited plasmon modes residing on coupled metal particles.

As this discussion has shown, Hamiltonians of the forms in Eqs. (1) and (7), in which hopping interactions between sites play an important role, serve as useful models for a

variety of physical systems. We refer to devices based on these types of interactions as "excitation" devices, and although we refer to the α_m as probability amplitudes, one should remain mindful that in certain contexts α_m may represent the classical amplitude of a field.

III. CONSERVATION OF EXCITATIONS AND EXCITATION CURRENTS

The Hamiltonians Eqs. (1) and (7) conserve excitation or particle number. The conservation of excitations is manifested in the behavior of the α_m. It is straightforward to show from Eq. (6) that

$$\frac{d|\alpha_m|^2}{dt} = \alpha_m^* \frac{d\alpha_m}{dt} + \alpha_m \frac{d\alpha_m^*}{dt} = -i \sum_n g_{mn}(\alpha_m^* \alpha_n - \alpha_n^* \alpha_m). \tag{14}$$

Summing both sides of this equation over all m yields

$$\frac{d}{dt} \sum_m |\alpha_m|^2 = 0. \tag{15}$$

The square of the magnitude of α_m is the probability of finding site m in the excited state. Equation (15) thus states that the probability of finding an excitation somewhere remains unchanged with time. In particular, in the single-particle sector of the Hilbert space, one has

$$\sum_m |\alpha_m|^2 = 1. \tag{16}$$

Given Eq. (15), it is natural to interpret the right-hand side of Eq. (14) as a probability current, namely the rate with which excitations flow to site m. Hence

$$J_{mn} = -i g_{mn}(\alpha_m^* \alpha_n - \alpha_n^* \alpha_m) \tag{17}$$

is the rate with which excitations flow from site n to site m.

IV. EXCITATION TRANSMISSION LINES

The energy coupling between nanoparticles in a chain can result in the waveguiding of excitation. In this section, an infinite chain of identical sites is considered. The nanoparticles, having frequency $\omega_m = \omega_0$, are linked by nearest neighbor interactions of the same strength: $g_{mn} = g$. This chain of sites forms a transmission line along which quanta can propagate. The dispersion relation for the excitation transmission line is now obtained. Let the sites be labeled with consecutive integers r indicating the position of a given site in the chain, and let the amplitude at the rth site be denoted by $\alpha_r(t)$. From Eq. (6), it follows that the time rate of change of the amplitude at the rth site is

$$i \frac{d\alpha_r}{dt} = \omega_0 \alpha_r + g(\alpha_{r-1} + \alpha_{r+1}). \tag{18}$$

When we write

$$\alpha_r = e^{-i(\omega t - \kappa r)}, \tag{19}$$

where κ is a unitless propagation constant for the quanta traveling over an equally spaced nanoparticle chain, and

$$\kappa = k_1 + i k_2, \tag{20}$$

where k_1 and k_2 are real, Eq. (18) yields the dispersion relation

$$\omega - \omega_0 = 2g[\cos(k_1)\cosh(k_2) - i \sin(k_1)\sinh(k_2)]. \tag{21}$$

Similar results have also been derived for coupled plasmon modes for a linear chain of equally spaced metal nanoparticles [14], which can be considered as a subset of the work presented here. For real frequencies ω and ω_0, Eq. (21) can only be satisfied if

$$\sin(k_1)\sinh(k_2) = 0. \tag{22}$$

Consideration of Eqs. (21) and (22) yields three classes of solutions. For

$$\frac{\omega - \omega_0}{2g} < -1, \tag{23}$$

Eq. (21) reduces to

$$\omega - \omega_0 = -2g \cosh(k), \tag{24}$$

obtained by setting $\cos(k_1) = -1$ and $k_2 = k$. The general solution to Eq. (18) at frequency ω in this case has the form

$$\alpha_r = (Ae^{-kr} + Be^{kr})e^{-i\omega t}, \tag{25}$$

where A and B are constants. For

$$-1 < \frac{\omega - \omega_0}{2g} < 1, \tag{26}$$

Eq. (21) reduces to

$$\omega - \omega_0 = 2g \cos(k), \tag{27}$$

obtained by setting $\sinh(k_2) = 0$ and $k_1 = k$. The general solution to Eq. (18) at frequency ω in this case has the form

$$\alpha_r = (Ae^{ikr} + Be^{-ikr})e^{-i\omega t}. \tag{28}$$

For

$$\frac{\omega - \omega_0}{2g} > 1, \tag{29}$$

Eq. (21) reduces to

$$\omega - \omega_0 = 2g \cosh(k), \tag{30}$$

obtained by setting $\cos(k_1) = 1$ and $k_2 = k$. The general solution to Eq. (18) at frequency ω in this case has the same form as Eq. (25):

$$\alpha_r = (Ae^{-kr} + Be^{kr})e^{-i\omega t}. \tag{31}$$

From Eq. (28), it is clear that the excitation transmission line supports traveling waves when

$$|\omega - \omega_0| < 2g. \tag{32}$$

Outside of this frequency range, the solutions grow or decay exponentially with respect to r. The focus here is on traveling wave solutions because they allow propagation of signals over large distances. However, even though signals at frequencies outside the range given by Eq. (32) decay exponentially away from the source, they can still be used to transmit information over short distances and may serve useful functions in excitation devices.

Restricting our attention to traveling wave solutions [Eq. (28)], the velocity with which signals travel along the

transmission line is given by the group velocity

$$v_g = \frac{\partial \omega_k}{\partial k}. \tag{33}$$

Note that this velocity has the unit of inverse time and indicates the rate with which a signal transferred from one site to the next. To convert this into a physical velocity, v_g must be multiplied by the distance between neighboring sites. From Eq. (27), one obtains

$$v_g = -2g \sin(k). \tag{34}$$

Note that when g is positive, the sign of the group velocity is opposite that of the phase velocity

$$v_p = \frac{\omega}{k}. \tag{35}$$

The magnitude of v_g takes on the maximum value

$$|v_g| = 2|g| \tag{36}$$

for

$$k = \pm\frac{\pi}{2}. \tag{37}$$

The set of distinct solutions of the form in Eq. (28) is obtained by restricting k to the range

$$0 < k < \pi. \tag{38}$$

We note that the general solution to Eq. (18) for propagating signals has the form

$$\alpha_r = \frac{1}{\sqrt{2\pi}} \int_0^{\pi} dk\, [A_R(k) e^{-i(\omega_k t - kx)} + A_L(k) e^{-i(\omega_k t + kx)}], \tag{39}$$

where the $A_R(k)$ and $A_L(k)$ are the amplitudes of components whose phase propagates, respectively, to the right or to the left. By changing the integration variable from k to ω and introducing the amplitudes

$$a_R(\omega) = \frac{1}{\sqrt{|v_g(\omega)|}} A_R(k) \tag{40}$$

and

$$a_L(\omega) = \frac{1}{\sqrt{|v_g(\omega)|}} A_L(k), \tag{41}$$

one obtains

$$\alpha_r(t) = \frac{1}{\sqrt{2\pi}} \int_{\omega_0 - 2|g|}^{\omega_0 + 2|g|} \frac{d\omega}{\sqrt{|v_g(\omega)|}} [a_R(\omega) e^{-i(\omega t - k_\omega r)} + a_L(\omega) e^{-i(\omega t + k_\omega r)}]. \tag{42}$$

A rationale for choosing the amplitudes in Eqs. (40) and (41) can be given by considering the excitation current flowing along the transmission line. From Eq. (17), the current flowing from site r to site $r+1$ is

$$J_{r+1,r} = -ig(\alpha_{r+1}^* \alpha_r - \alpha_r^* \alpha_{r+1}). \tag{43}$$

By substituting Eq. (42) into Eq. (43) and integrating both sides of Eq. (43) over all time, we obtain

$$\int_{-\infty}^{\infty} J_{r+1,r} dt = -\mathrm{sgn}(g) \times \int_{\omega_0 - 2|g|}^{\omega_0 + 2|g|} d\omega [a_R^*(\omega) a_R(\omega) - a_L^*(\omega) a_L(\omega)], \tag{44}$$

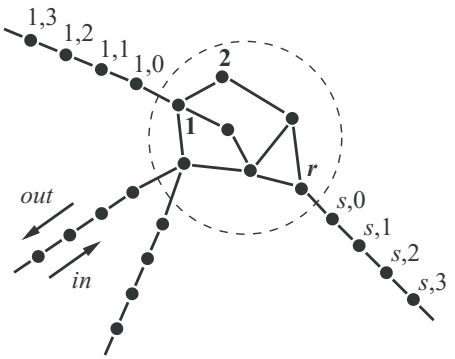

FIG. 1. Excitation device (in dashed circle) connected to hopping transmission lines.

where $\mathrm{sgn}(g)$ denotes the sign of g. It is apparent that $a_R^*(\omega) a_R(\omega)$ and $a_L^*(\omega) a_L(\omega)$ correspond to the power spectral density of the excitation current for excitations with right-going and left-going phase velocities, respectively.

V. GENERAL FORMULAS FOR DEVICE SYNTHESIS

In addition to the waveguides shown in Sec. IV, networks of nanoparticles can be constructed that realize any discrete unitary transformation on the input modes. In this section, formulas for general nanoparticle network shown in Fig. 1 are derived.

The network within the circle constitutes an excitation device. The sites are located at the nodes of the network, and the edges of the network indicate which sites are coupled via hopping interactions. The excitation device is connected to excitation transmission lines, which are indicated as linear chains of sites outside the circle. The sites within the circle are labeled with integers 1 through N where N is the number of sites contained within the device. The transmission line sites are labeled by a pair of numbers, the first of which indicates the transmission line number and ranges from 1 to M where M is the total number of transmission lines. The second number is an integer that, starting from zero, successively increments as one moves from site to site away from the device. In particular, in the figure, site r has transmission line s attached to it, and successive sites along the transmission line are labeled $(s,0)$, $(s,1)$, $(s,2)$, ... The transmission lines carry signals that propagate "in" toward the device or "out" away from the device.

One would like to solve for the outgoing signals in terms of the incoming signals in order to identify devices that perform useful transformations on incoming signals. To perform such an analysis, it is useful to distinguish three classes of sites. The first class consists of those sites belonging to the device. From Eq. (6), the amplitudes at these sites satisfy

$$i\frac{d\alpha_r}{dt} = \omega_r \alpha_r + \sum_{r'} g_{r,r'} \alpha_{r'} + \sum_s g_{r,s0} a_{s,0}, \tag{45}$$

where $g_{r,s0}$ is the strength of the hopping interaction between device site r and the first site of transmission line s. (The second sum need not be present for all nodes, because some device sites need not be connected directly to a transmission line.) Note that we are allowing for the possibility that more

than one transmission line is connected to the same node. The second class of sites consists of the first site of each transmission line. The amplitudes at these sites satisfy

$$i\frac{d\alpha_{s,0}}{dt} = \omega_s\alpha_{s,0} + g_{r,s0}\alpha_r + g_s\alpha_{s,1}, \tag{46}$$

where g_s is the hopping interaction strength between nearest neighbors along transmission line s. The third class of sites consists of those interior to the transmission line. These satisfy

$$i\frac{d\alpha_{s,m}}{dt} = \omega_s\alpha_{s,m} + g_s(\alpha_{s,m+1} + \alpha_{s,m-1}), \tag{47}$$

where $m > 0$.

It is most convenient to work in frequency space. To this end, we introduce the following Fourier decomposition for the α_r:

$$\alpha_r(t) = \frac{1}{\sqrt{2\pi}}\int_{-\infty}^{\infty} d\omega\, a_r(\omega)e^{-i\omega t}. \tag{48}$$

We follow Eq. (42) for the Fourier decomposition of the amplitudes $\alpha_{r,m}$ along the transmission lines. To simplify the discussion, we restrict ourselves to the case when $g > 0$. In this case, the group velocity [Eq. (34)] is opposite that of the phase velocity. Hence, we write

$$\alpha_{r,m} = \frac{1}{\sqrt{2\pi}}\int_{\omega_0-2g_r}^{\omega_0+2g_r}\frac{d\omega}{\sqrt{|v_{gr}(\omega)|}}\left[a_r^{\text{in}}(\omega)e^{-i(\omega t-k_\omega m)} + a_r^{\text{out}}(\omega)e^{-i(\omega t+k_\omega m)}\right], \tag{49}$$

where the "in" and "out" superscripts indicate whether the signal is propagating toward or away from the device. For the case when g is negative, the "in" and "out" labels have to be interchanged, and the overall sign of the expression on the right-hand side of Eq. (46) has to be changed as well.

To further simplify the analysis, we restrict ourselves to the study of frequency components that fall within the passbands of all the transmission lines. In this case, in terms of the frequency components of Eqs. (48) and (49), Eqs. (45) and (46) become

$$(\omega-\omega_r)a_r(\omega) = \sum_{r'} g_{r,r'}a_{r'}(\omega) + \sum_s \frac{g_{r,s0}}{\sqrt{|v_{gs}(\omega)|}} \times \left[a_s^{\text{in}}(\omega) + a_s^{\text{out}}(\omega)\right] \tag{50}$$

and

$$\frac{(\omega-\omega_s)}{\sqrt{|v_{gs}(\omega)|}}\left[a_s^{\text{in}}(\omega) + a_s^{\text{out}}(\omega)\right] = g_{r,s0}a_r(\omega) + \frac{g_s}{\sqrt{|v_{gs}(\omega)|}}\left[a_s^{\text{in}}(\omega)e^{ik_\omega} + a_s^{\text{out}}(\omega)e^{-ik_\omega}\right]. \tag{51}$$

Equation (47) is already satisfied by Eq. (50) and need not concern us further. For device characterization, we would like to solve this system of equations for the $a_s^{\text{out}}(\omega)$ in terms of the $a_s^{\text{in}}(\omega)$. Solving Eq. (51) for $a_s^{\text{out}}(\omega)$ yields

$$a_s^{\text{out}}(\omega) = \frac{\sqrt{|v_{gs}(\omega)|}g_{r,s0}}{\omega-\omega_s-g_se^{-ik_\omega}}a_r(\omega) - \frac{\omega-\omega_s-g_se^{ik_\omega}}{\omega-\omega_s-g_se^{-ik_\omega}}a_s^{\text{in}}(\omega). \tag{52}$$

This can be used to eliminate the $a_s^{\text{out}}(\omega)$ from Eq. (50). Equation (50) can then be solved for the $a_r(\omega)$ in terms of $a_s^{\text{in}}(\omega)$. Once the $a_r(\omega)$ have been determined, they can be substituted in Eq. (52) to determine the outgoing fields. Because the set of Eqs. (50) and (51) is linear, the relation between the $a_s^{\text{out}}(\omega)$ and the $a_s^{\text{in}}(\omega)$ can be written in scattering matrix form as

$$\begin{pmatrix} a_1^{\text{out}}(\omega) \\ a_2^{\text{out}}(\omega) \\ \cdot \\ \cdot \\ \cdot \end{pmatrix} = \begin{pmatrix} S_{11}(\omega) & S_{12}(\omega) & \cdots \\ S_{21}(\omega) & S_{22}(\omega) & \cdots \\ \cdot & \cdot & \\ \cdot & \cdot & \\ \cdot & \cdot & \end{pmatrix} \begin{pmatrix} a_1^{\text{in}}(\omega) \\ a_2^{\text{in}}(\omega) \\ \cdot \\ \cdot \\ \cdot \end{pmatrix}. \tag{53}$$

Because the system conserves excitation number and because the $a_s^{\text{in}}(\omega)$ and $a_s^{\text{out}}(\omega)$ have been normalized so that their magnitudes squared represent the power spectral density of the excitation current, the scattering matrix

$$\mathbf{S} = \begin{pmatrix} S_{11}(\omega) & S_{12}(\omega) & \cdots \\ S_{21}(\omega) & S_{22}(\omega) & \cdots \\ \cdot & \cdot & \\ \cdot & \cdot & \\ \cdot & \cdot & \end{pmatrix} \tag{54}$$

is unitary.

VI. BEAM SPLITTER

In this section, an excitation beam splitter is described using the formulation derived in Sec. V. An excitation beam splitter can be regarded as analogous to a radio frequency hybrid coupler constructed from sections of quarter-wave transmission lines [41]. The device is depicted in Fig. 2. The labeling of the device and transmission line nodes are indicated in this figure, as are the hopping interaction coupling strengths between the various nodes.

Considering the case where all the site frequencies ω_r are equal to ω_0, the set of equations corresponding to Eq. (50) for this device is

$$(\omega-\omega_0)a_1(\omega) = g_2a_2(\omega) + g_1a_3(\omega) + \frac{g}{\sqrt{|v_g(\omega)|}}\left[a_1^{\text{in}}(\omega) + a_1^{\text{out}}(\omega)\right], \tag{55}$$

$$(\omega-\omega_0)a_2(\omega) = g_2a_1(\omega) + g_1a_4(\omega) + \frac{g}{\sqrt{|v_g(\omega)|}}\left[a_2^{\text{in}}(\omega) + a_2^{\text{out}}(\omega)\right], \tag{56}$$

$$(\omega-\omega_0)a_3(\omega) = g_2a_4(\omega) + g_1a_1(\omega) + \frac{g}{\sqrt{|v_g(\omega)|}}\left[a_3^{\text{in}}(\omega) + a_3^{\text{out}}(\omega)\right], \tag{57}$$

and

$$(\omega-\omega_0)a_4(\omega) = g_2a_3(\omega) + g_1a_2(\omega) + \frac{g}{\sqrt{|v_g(\omega)|}}\left[a_1^{\text{in}}(\omega) + a_1^{\text{out}}(\omega)\right]. \tag{58}$$

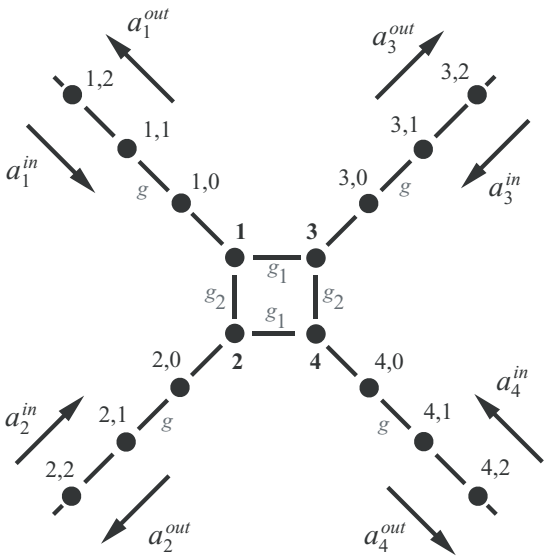

FIG. 2. Beam splitter for excitations. The device nodes are labeled with the integers 1 through 4. The transmission line nodes are indicated by pairs of numbers r, m where the first labels the transmission line and the second labels a node along that transmission line. The hopping interaction coupling strengths between pairs of nodes within the device are labeled by g_n, where n is 1 or 2. The hopping interaction coupling strengths between neighboring nodes along the transmission lines are all taken to be equal to g. The direction of propagation of the incoming a_r^{in} and outgoing a_r^{out} amplitudes for each of the transmission lines is also indicated.

Equation (52) for the rth transmission line becomes

$$a_r^{\text{out}}(\omega) = \frac{\sqrt{|v_g(\omega)|}g}{\omega - \omega_0 - ge^{-ik_\omega}} a_r(\omega) - \frac{\omega - \omega_0 - ge^{ik_\omega}}{\omega - \omega_0 - ge^{-ik_\omega}} a_r^{\text{in}}(\omega), \tag{59}$$

where $r = 1, 2, 3, 4$. Of particular interest here is the case when ω is the midband frequency ω_0. From the dispersion relation [Eq. (27)], it follows that at this frequency $k = \pi/2$. By imposing the further restriction

$$g_1^2 = g^2 + g_2^2 \tag{60}$$

and introducing

$$K = \frac{g}{g_1}, \tag{61}$$

Eqs. (55) through (59) yield the scattering matrix

$$\mathbf{S}(\omega_0) = \begin{pmatrix} 0 & 0 & iK & \sqrt{1-K^2} \\ 0 & 0 & \sqrt{1-K^2} & iK \\ iK & \sqrt{1-K^2} & 0 & 0 \\ \sqrt{1-K^2} & iK & 0 & 0 \end{pmatrix} \tag{62}$$

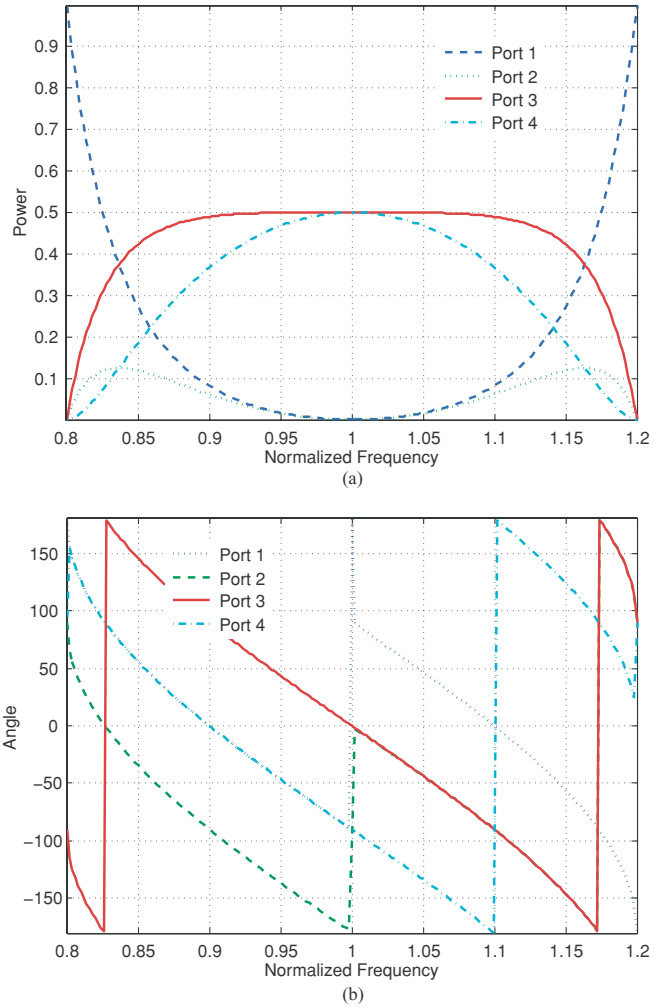

FIG. 3. (Color online) Power transferred to each port (a) and the corresponding phase (b) as a function of normalized frequency for the 50:50 beam splitter described in Fig. 2. The input from port 1 is evenly split in power between ports 3 and 4 at normalized frequency of 1. A 3-dB bandwidth in the unit of $0.2\omega_0$ is achieved. The phase difference between the two ports is 90°.

for which

$$\begin{pmatrix} a_1^{\text{out}}(\omega_0) \\ a_2^{\text{out}}(\omega_0) \\ a_3^{\text{out}}(\omega_0) \\ a_4^{\text{out}}(\omega_0) \end{pmatrix} = \mathbf{S}(\omega_0) \begin{pmatrix} a_1^{\text{in}}(\omega_0) \\ a_2^{\text{in}}(\omega_0) \\ a_3^{\text{in}}(\omega_0) \\ a_4^{\text{in}}(\omega_0) \end{pmatrix}. \tag{63}$$

It is apparent that a signal entering input port 1 or 2 is only delivered to output ports 3 and 4. Likewise, a signal entering input port 3 or 4 is only delivered to output ports 1 and 2. Hence, the device functions like a beam splitter. The functionality of a 50:50 beam splitter (or 3-dB coupler) is achieved when $K = 1/\sqrt{2}$. This occurs, for example, when $g_1 = \sqrt{2}g$ and $g_2 = g$. Plots of the square magnitudes of the scattering matrix for this beam splitter, at frequencies away from ω_0, is shown in Fig. 3.

Assuming that the incident signal enters the beam splitter from port 1, the output is evenly split between ports 3 and 4 with a normalized 3-dB bandwidth of 0.2. In the calculation,

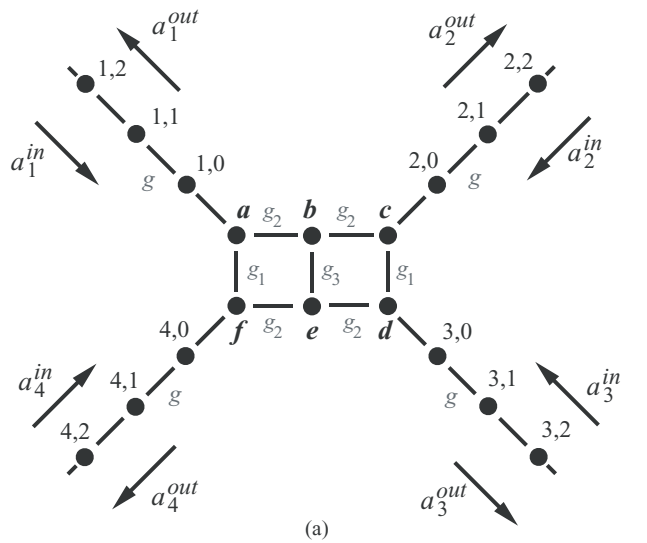

(a)

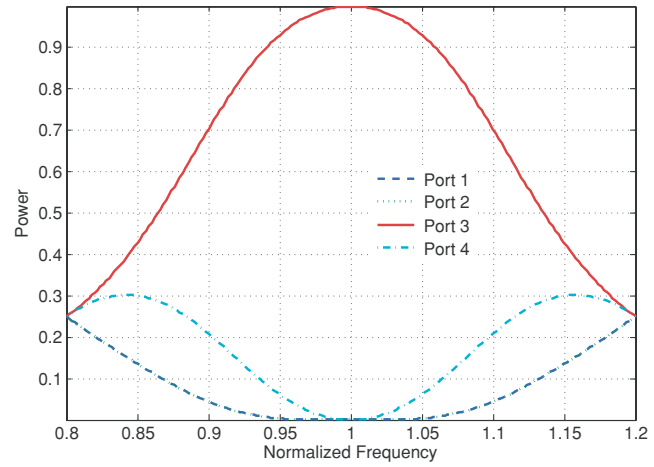

(b)

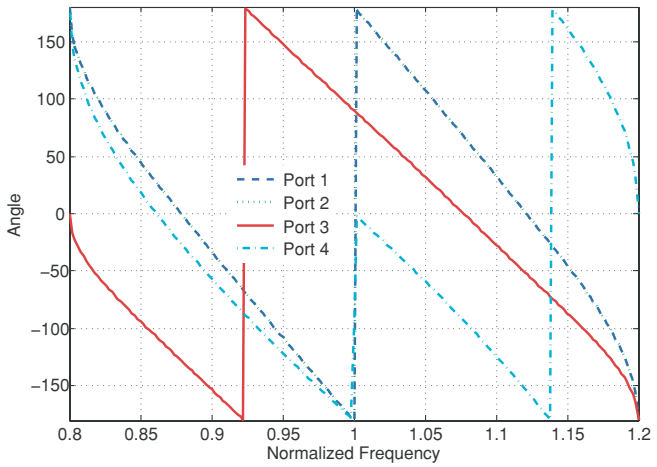

(c)

FIG. 4. (Color online) (a) Schematic of a crossover splitter. The coupling strength between the adjacent nanoparticles is labeled on the transmission line connecting the nanoparticles. The power transferred to each port (b) and the corresponding phase (c) are calculated as a function of normalized frequency. The input from port 1 is transmitted to port 3 with an efficiency of 100% at the normalized frequency of 1. The phase difference between the input and output is 90° at the same frequency. The plot for port 2 overlaps with that of port 1 in the figure.

the coupling strengths are $g_2 = g = 0.10$ and $g_1 = 0.14$. If the coupling strength g_2 between nodes 1 and 2 and between nodes 3 and 4 were to increase simultaneously by the same amount, a greater signal magnitude will emerge from output port 4 than from output port 3. Conversely, greater signal output from port 3 than from port 4 is expected when the coupling strength is reduced between nodes 1 and 2 and between nodes 3 and 4. For the former, it also gives rise to an increased reflection from port 1. For the latter, it leads to an increase in transmitted power to the output port 2 while the reflection to port 1 is largely unchanged. In practice, this modification of coupling strength can be achieved by physically reducing the distance between the nanoparticles, a change of dielectric constant in the vicinity of the nanoparticles, or through external sources.

VII. CROSSOVER DEVICE FOR EXCITATIONS

Another useful device that can be achieved with nanoscale photonics is a crossover splitter. Figure 4(a) shows an example of such a device. The four input/output ports are connected through a junction consisting of six nanoparticles labeled as a–f. Through resonant coupling among the nanoparticles, this planar device allows the input from port 1 to be channeled to the opposing port, port 3. All nanoparticles shown in Fig. 4(a) have a normalized resonant frequency of 1. The coupling strengths between the adjacent nanoparticles are labeled on the transmission lines connecting the nanoparticles.

The crossover splitter can be viewed as a two 50:50 beam splitters, of the type as shown in Fig. 2, in cascade. Figure 4(b) shows the power-transfer efficiency for the device and the corresponding phase at the output port as a function of normalized frequency. In the calculation, the coupling strengths are $g_1 = g = 0.10$, $g_2 = 0.14$, and $g_3 = 0.20$. The energy-transfer efficiency at the normalized frequency of 1 is 100%. The normalized bandwidth of 3-dB power transfer is approximately 0.25.

Further, through a lengthy but straightforward analysis, similar to that done to obtain Eq. (62), it can be shown that the crossover splitter can always deliver 100% power transfer as long as the coupling strength g_2 among a, b, and c and

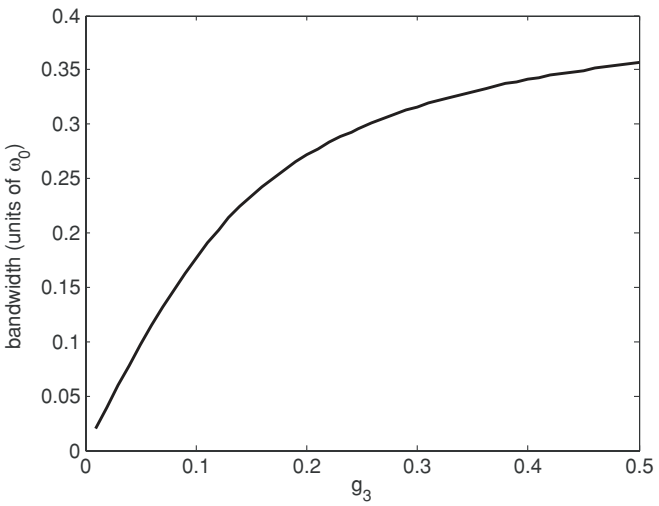

FIG. 5. Bandwidth of the crossover splitter as a function of coupling strength g_3, in units of ω_0.

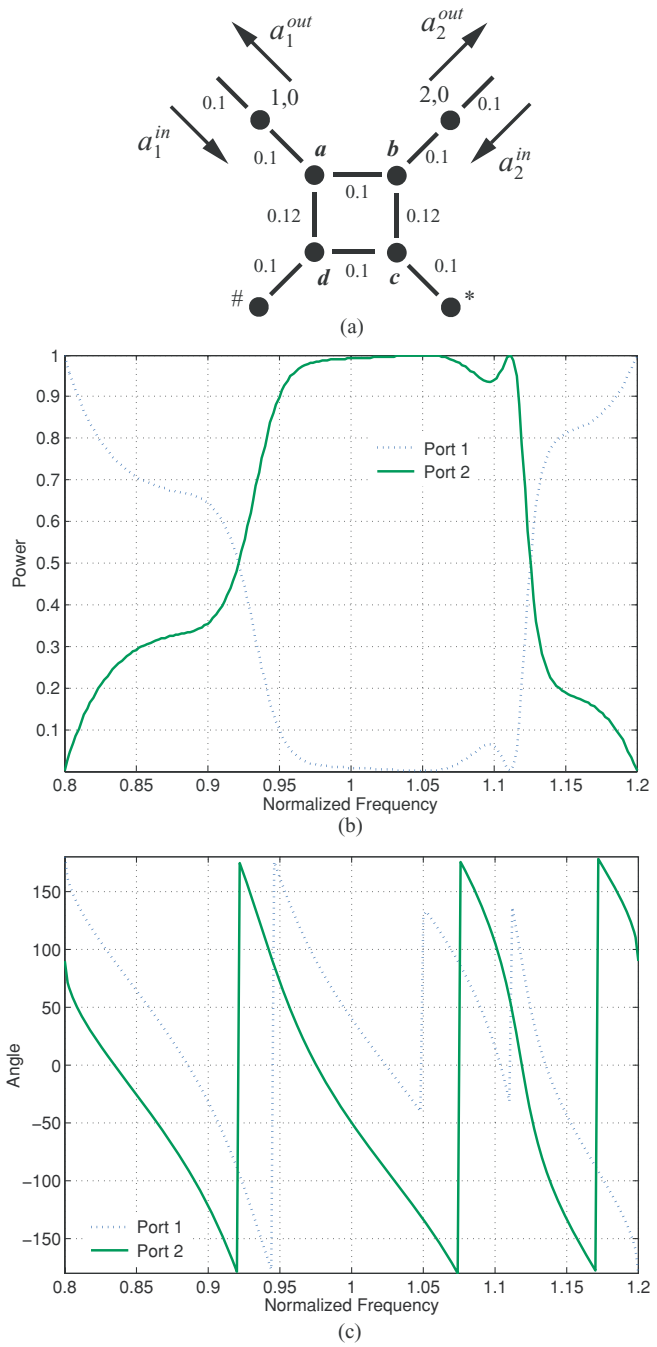

FIG. 6. (Color online) (a) Schematic of a phase shifter consisting of a modified 50:50 beam splitter with two detuned nanoparticles. (b) Reflected power from port 1 and the transmitted power to port 2 as a function of normalized frequency. (c) Phase-frequency relation for the reflection from port 1 and the transmission to port 2. The power incident from port 1 shifted in phase by 50° when it exits port 2. The output intensity is nearly unchanged for a bandwidth in the unit of 0.1 ω_0.

among d, e, and f; coupling strength g_3 between b and e; and the remaining coupling strength g_1 satisfy the following relationship:

$$g_2 = \sqrt{g_1 g_3}. \tag{64}$$

Under this condition, the bandwidth for 3-dB power transfer can be calculated as a function of g_3. Figure 5 shows that the bandwidth always increases with a stronger coupling. In practice, the coupling strength is limited by the fabrication capability, for example, the minimum distance where the nanoparticles can be reliably placed, and other nonradiative loss.

VIII. PHASE SHIFTER

As a final example of a nanophotonic device constructed from nanoparticles, a phase shifter is shown in Fig. 6(a). The phase shifter is a two-port network derived from the 50:50 beam splitter, shown in Fig. 2, by replacing the transmission lines of ports 3 and 4 with two nanoparticles whose resonant frequency is slightly detuned from the rest of the nanoparticle network.

In Fig. 6(b) and 6(c), the intensity and phase at the output port 2 are shown as functions of frequency. The detuning nanoparticles, labeled as $*$ and #, have a normalized resonant frequency of 1.05. The coupling strength between the adjacent nanoparticles is labeled on the corresponding link. In this case, the phase shift experienced at output port 2 is 310° at a normalized frequency of 1. The amount of phase shift is controlled by either the coupling strengths between a and d and between b and c or the detuning frequency. Increasing these values leads to an increase of phase shift. However, an increase of detuning frequency leads to a decrease of transmitted power at output port 2.

IX. DISCUSSION AND CONCLUSIONS

The networks of nanoparticles described in this article are characterized by normalized coupling strengths between the neighboring nanoparticles for the sake of generality. It is necessary to make a brief discussion on its value in a practical system. As shown in Sec. II, the discussion of excitation transfer also applies for plasmons coupling in a chain of metal particles. Considering coupled plasmon modes in a metal nanoparticle chain, for instance, the interaction between adjacent nanoparticles is dominantly the near field coupling. By approximating the plasmon mode on each metal nanoparticle as a Hertzian dipole, we give the coupling strength as $\sqrt{qe/4\pi m\varepsilon_0 n^2 d^3}$ [42], where q is the magnitude of the oscillating charges, m is electron mass, n is the refractive index of the dielectric surrounding the metal nanoparticles, and d is the distance between the adjacent nanoparticles. For an array of 10-nm-diameter Ag particles in vacuum, the coupling strength is 4×10^{14} rad/s when they are spaced by 35 nm. For the resonant frequency ω_m of 3×10^{15} rad/s, or 0.6 μm, the normalized coupling strength is approximately 0.1. It is worth noting that a small change in distance can significantly modify the coupling strength since it is $-3/2$ power of the distance. For example, the normalized coupling strength increases to 0.14 when the distance between the adjacent nanoparticles is reduced by 6 nm. Hence, an accurate control of fabrication with nanometer precision is required for such devices.

In conclusion, a generic formulism is presented for the design of passive lossless linear devices from components interacting via hopping interactions. A nanoparticle network was presented as a solution for sub-diffraction-limit energy propagation. We have also illustrated the use of this formalism

for constructing functional optical devices, such as beam splitters, phase shifters, and crossover splitters. These three components are primatives, from which networks performing a given unitary transformation can be constructed. Notably, all the components of these networks can lie in the same plane, a feature that is particularly convenient when devices are fabricated on a planar surface.

ACKNOWLEDGMENTS

The authors gratefully acknowledge the support from the Defense Advanced Research Projects Agency (DARPA) Microsystems Technology Office (MTO) under Contract No. N66001-05-1-8911 and from the National Science Foundation (NSF) under Grant Nos. CCF-0855212, CAREER ECCS-0846415, and MRI-0923541 for this work.

[1] C.-J. Wang and L. Y. Lin, Nanoscale Res. Lett. **2**, 219 (2007).
[2] M. F. García-Parajó, J. Hernando, G. Sanchez Mosteiro, J. P. Hoogenboom, E. M. H. P. van Dijk, and N. F. van Hulst, ChemPhysChem **6**, 819 (2005).
[3] A. Alù and N. Engheta, Phys. Rev. B **79**, 235412 (2009).
[4] A. Alù and N. Engheta, Phys. Rev. B **75**, 024304 (2007).
[5] A. Alù and N. Engheta, Phys. Rev. B **74**, 205436 (2006).
[6] A. F. Koenderink and A. Polman, Phys. Rev. B **74**, 033402 (2006).
[7] R. A. Shore and A. D. Yaghjian, Electron. Lett. **41**, 578 (2005).
[8] R. A. Shore and A. D. Yaghjian, IEICE Trans. Commun. **E88-B**, 2346 (2005).
[9] W. H. Weber and G. W. Ford, Phys. Rev. B **70**, 125429 (2004).
[10] S. A. Maier *et al.*, Nat. Mater. **2**, 229 (2003).
[11] S. A. Maier, M. L. Brongersma, and H. A. Atwater, Appl. Phys. Lett. **78**, 16 (2001).
[12] M. Quinten *et al.*, Opt. Lett. **23**, 1331 (1998).
[13] M. Sukharev and T. Seideman, J. Phys. B **40**, S283 (2007).
[14] M. L. Brongersma, J. W. Hartman, and H. A. Atwater, Phys. Rev. B **62**, R16356 (2000).
[15] Y. Kubota and K. Nobusada, J. Chem. Phys. **129**, 094704 (2008).
[16] S.-K. Hong *et al.*, Phys. Lett. **A360**, 1 (2006).
[17] S. Sangu, K. Kobayashi, A. Shojiguchi, and M. Ohtsu, Phys. Rev. B **69**, 115334 (2004).
[18] S. Sangu *et al.*, J. Appl. Phys. **93**, 2937 (2003).
[19] C.-J. Wang, B. A. Parviz, and L. Y. Lin, Nanotechnology **19**, 295201 (2008).
[20] C.-J. Wang *et al.*, Nano Lett. **6**, 2549 (2006).
[21] D. Beljonne *et al.*, J. Phys. Chem. B **113**, 6583 (2009).
[22] G. Sánchez-Mosteiro *et al.*, J. Phys. Chem. B **110**, 26349 (2006).
[23] P. Tinnefeld, M. Heilemann, and M. Sauer, ChemPhysChem **6**, 217 (2005).
[24] S. Vyawahare *et al.*, Nano Lett. **4**, 1035 (2004).
[25] S. Jang *et al.*, J. Chem. Phys. **129**, 101104 (2008).
[26] S. Jang, M. D. Newton, and R. J. Silbey, J. Phys. Chem. B **111**, 6807 (2007).
[27] A. Kimura and T. Kakitani, J. Phys. Chem. A **111**, 12042 (2007).
[28] A. V. Pisliakov, T. Mançal, and G. R. Fleming, J. Chem. Phys. **124**, 234505 (2006).
[29] S. Jang, M. D. Newton, and R. J. Silbey, Phys. Rev. Lett. **92**, 218301 (2004).
[30] A. Kimura and T. Kakitani, J. Phys. Chem. B **107**, 14486 (2003).
[31] J. A. Leegwater, J. Phys. Chem. **100**, 14403 (1996).
[32] V. M. Kenkre and R. S. Knox, Phys. Rev. B **9**, 5279 (1974).
[33] G. S. Engel *et al.*, Nature **446**, 782 (2007).
[34] D. Zigmantas *et al.*, PNAS **103**, 12672 (2006).
[35] T. Brixner *et al.*, Nature **434**, 625 (2005).
[36] E. Collini and G. D. Scholes, Science **323**, 369 (2009).
[37] J. Cai and G. D. Mahan, Phys. Rev. B **76**, 205116 (2007).
[38] R. Wang, J. Wang, and J.-Q. Liang, Physica B **387**, 172 (2007).
[39] M. Reck, A. Zeilinger, H. J. Bernstein, and P. Bertani, Phys. Rev. Lett. **73**, 58 (1994).
[40] Greiner, *Classical Electrodynamics* (Springer-Verlag, New York, 1996).
[41] K. W. Eccleston and S. H. M. Ong, IEEE Trans. Microwave Theory Tech. **51**, 2119 (2003).
[42] J. D. Jackson, *Classical Electrodynamics* (Wiley, New York, 1999).